Arctic (2) also exhibited high growth rates and have been placed at approximately 75° to 80°N paleolatitude (8). These deposits had ring widths averaging 3.0 to 5.0 mm with a maximum of 10 mm (based on field measurements). In the Arctic today, trees are capable of producing a growth ring in as little as one month. Cambial activity in many of these trees ceases even though light levels still appear to be adequate for photosynthetic activity. This growth pattern suggests that modern high-latitude trees are limited by temperature; the narrow size of their rings (1.0 mm or less) supports this interpretation. Temperature does not appear to have been a limiting factor to forest growth during the Late Permian in Antarctica. The deciduous nature of the *Glossopteris* forest, combined with the relatively large size of the growth rings, suggests that the climate was more favorable to tree growth than that which occurs today at latitudes 10° to 15° lower. On the basis of the rate of tree growth, the Permian polar climate is more comparable to Paleocene-Eocene climates in the Arctic.

As is true of temperate trees today, there was a clear cessation of cambial activity each year in these Permian trees. The small proportion of latewood suggests that cambial activity suddenly ceased at the end of the growing season, which otherwise appeared to be quite favorable for growth. In the absence of frost rings, we suggest that latewood production and the subsequent cessation of cell divisions in the vascular cambium were a response to decreasing light levels in the autumn. Basinger (2) has proposed that minimal latewood development in the Paleocene Arctic woods indicates a lack of winter hardening in these plants. He suggested that these trees experienced only short periods of freezing weather, if any.

Some models, based primarily on physical parameters, have suggested that winter temperatures averaged −30° to −40°C and summer temperatures 0°C for this region [for example (8)]. However, the biological evidence suggests that this was not the case. Clearly, Permian forests were present at latitudes where no vascular plants can survive today. Growth in these forests could be extremely fast, as evidenced by growth ring data. A lack of latewood development in the tree rings and the absence of frost rings suggests that temperatures rarely went below freezing.

Biological input to physical climate models is of primary importance in limiting the range of past climatic interpretations and can provide increased resolution when integrated with such models. More importantly, these data provide important information that can be applied to expand our knowledge of possible changes in plant growth and distribution as a result of current climate changes.

REFERENCES AND NOTES

1. T. H. Jefferson, *Palaeontology* **25**, 681 (1982).
2. J. E. Francis, *Arctic* **41**, 314 (1988); J. E. Francis, *Geol. Surv. Can. Bull.* **403**, 29 (1991); J. F. Basinger, *ibid.*, p. 39.
3. J. L. Isbell, thesis, Ohio State University (1990). The site was first noted by Isbell during the 1985 and 1986 field season. The sedimentology of Mount Achernar and other Buckley Formation sites in the central Transantarctic Mountains are discussed in this thesis.
4. N. R. Cúneo, J. L. Isbell, E. L. Taylor, T. N. Taylor, *C. R. XII Int. Congr. Carb. and Permian Geo. Strat.*, Buenos Aires, Argentina, 22 to 27 September 1991, S. Archangelsky, Ed., Buenos Aires (in press).
5. M. J. Farabee, E. L. Taylor, T. N. Taylor, *Rev. Palaeobot. Palynol.* **69**, 353 (1991).
6. G. J. Retallack, *Bull. Geol. Surv. New South Wales* **26**, 384 (1980); B. M. Gunn and R. I. Walcott, *N. Z. J. Geol. Geophys.* **5**, 407 (1962).
7. R. A. Spicer and J. L. Chapman, *Trends Ecol. Evol.* **5**, 279 (1990); J. A. Wolfe, *Paleobiology* **13**, 215 (1987); D. I. Axelrod, *Evolution* **20**, 1 (1966).
8. E. Irving and P. J. Wynne, *Geol. Surv. Can. Bull.* **403**, 209 (1991).
9. T. J. Crowley, W. T. Hyde, D. A. Short, *Geology* **17**, 457 (1989); J. E. Kutzbach and R. G. Gallimore, *J. Geophys. Res.* **94**, 3341 (1989).

10. This work was supported in part by the National Science Foundation (DPP-8815976 to T.N.T. and E.L.T. and DPP-9109448 to E.L.T.) and by an Ohio State University Byrd Fellowship to N.R.C. We thank J. L. Isbell and J. W. Collinson for helpful comments on the manuscript and J. L. Isbell for field assistance. E.L.T. also thanks the members of the Laboratory of Tree-Ring Research, University of Arizona, Tucson, for assistance with tree-ring analysis techniques and helpful discussions. Contribution no. 810 of the Byrd Polar Research Center.

14 May 1992; accepted 22 July 1992

Structural Models for the Metal Centers in the Nitrogenase Molybdenum-Iron Protein

Jongsun Kim and D. C. Rees*

Structural models for the nitrogenase FeMo-cofactor and P-clusters are proposed based on crystallographic analysis of the nitrogenase molybdenum-iron (MoFe)-protein from *Azotobacter vinelandii* at 2.7 angstrom resolution. Each center consists of two bridged clusters; the FeMo-cofactor has 4Fe:3S and 1Mo:3Fe:3S clusters bridged by three non-protein ligands, and the P-clusters contain two 4Fe:4S clusters bridged by two cysteine thiol ligands. Six of the seven Fe sites in the FeMo-cofactor appear to have trigonal coordination geometry, including one ligand provided by a bridging group. The remaining Fe site has tetrahedral geometry and is liganded to the side chain of $Cys^{\alpha 275}$. The Mo site exhibits approximate octahedral coordination geometry and is liganded by three sulfurs in the cofactor, two oxygens from homocitrate, and the imidazole side chain of $His^{\alpha 442}$. The P-clusters are liganded by six cysteine thiol groups, two which bridge the two clusters, α88 and β95, and four which singly coordinate the remaining Fe sites, α62, α154, β70, and β153. The side chain of $Ser^{\beta 188}$ may also coordinate one iron. The polypeptide folds of the homologous α and β subunits surrounding the P-clusters are approximately related by a twofold rotation that may be utilized in the binding interactions between the MoFe-protein and the nitrogenase Fe-protein. Neither the FeMo-cofactor nor the P-clusters are exposed to the surface, suggesting that substrate entry, electron transfer, and product release must involve a carefully regulated sequence of interactions between the MoFe-protein and Fe-protein of nitrogenase.

Reduction of dinitrogen to ammonia by the nitrogenase enzyme system requires two metalloproteins, the molybdenum-iron (MoFe)–protein and the iron (Fe)–protein [reviewed in (*1*)]. The MoFe-protein is an $\alpha_2\beta_2$ tetramer with total molecular mass of ~240 kD, and the Fe-protein is a γ2 dimer. Three distinct types of redox centers are associated with these proteins: The MoFe-protein contains two types of centers, the FeMo-cofactor [reviewed in (*2*)] and the P-clusters [reviewed in (*3*)], and the Fe-protein dimer contains one 4Fe:4S cluster whose structure is described in an accompanying article (*4*). Because the active site of nitrogenase is provided by the MoFe-protein, the redox centers of this protein have attracted considerable attention. The FeMo-cofactor, first identified by Shah and Brill (*5*), most likely represents the site of substrate reduction (*6*) and has the approximate composition of one Mo atom, six to eight Fe atoms, eight to nine S atoms, and one homocitrate group (1Mo:6-8Fe:8-9S:1 homocitrate) (*2*, *7*, *8*). The P-clusters are believed to contain two 4Fe:4S clusters in close proximity (*9*–*13*), although the detailed properties of this center are distinct from better characterized proteins that con-

Division of Chemistry and Chemical Engineering 147-75CH, California Institute of Technology, Pasadena, CA 91125.

*To whom correspondence should be addressed.

tain one or more mononuclear 4Fe:4S clusters. The overall metal composition of the MoFe-protein, approximately 2Mo:30Fe:30S, is consistent with the presence of two copies each of the FeMo-cofactor and P-clusters per MoFe-protein tetramer. Despite extensive study, the detailed structures of the FeMo-cofactor and P-clusters have not yet been established. In this report, structural models for the FeMo-cofactor and P-clusters, based on crystallographic analysis at 2.7 Å resolution of the MoFe-protein from *Azotobacter vinelandii*, are presented. Each center consists of two bridged clusters; the FeMo-cofactor has 4Fe:3S and 1Mo:3Fe:3S clusters bridged by three nonprotein ligands, whereas the P-clusters contain two 4Fe:4S clusters bridged by two cysteine thiol ligands.

The MoFe-protein crystal structure was determined by the methods of multiple isomorphous replacement (MIR) and noncrystallographic symmetry (NCS) averaging within and between crystal forms. Three crystal forms of MoFe-protein, purified by protocols modified from (*14*) and (*7*) for the MoFe-proteins from *A. vinelandii* and *Clostridium pasteurianum*, respectively, were used in the structure determination. The *A. vinelandii* MoFe-protein (designated Av1) was crystallized by the microcapillary batch method (*15*) from 18% polyethylene glycol (PEG) 4000, 0.14 M NaCl, 0.10 M Na_2MoO_4, 80 mM tris-HCl, pH 8.0, and ~8 mg/ml protein. Two crystal forms of the *C. pasteurianum* MoFe-protein (designated Cp1) were obtained by crystallization from 15% PEG 4000, 0.21 M $MgCl_2$, 80 mM tris HCl, pH 8.0, and ~8 mg/ml protein (crystal form designated Mg1) and by crystallization from 18% PEG 4000, 0.3 M CsCl, and 80 mM tris HCl, pH 8.0, and ~8 mg/ml protein (designated Cs1). All three crystal forms belong to space group $P2_1$, with cell constants a = 108.4 Å, b = 130.5 Å, c = 81.5, β = 110.8°; a = 70.0 Å, b = 151.3 Å, c = 121.9 Å, β = 110.4°; and a = 87.9 Å, b = 171.4 Å, c = 73.6 Å, β = 91.5°, for the Av1, Mg1, and Cs1 forms, respectively. Each form contains one $\alpha_2\beta_2$ tetramer per asymmetric unit. The Mg1 form is similar to a crystal form previously described (*16*). Diffraction data were collected at room temperature on a Siemens multiwire area detector and processed (Table 1) with XENGEN (*17*). Heavy atom derivatives of Av1 were prepared by soaking separate crystals in solutions of 5 mM ethylmercurithiosalicylate (EMTS), 5 mM K_2PtCl_4, and 4 mM di-μ-iodobis(ethylenediamine)-di-platinum (II) nitrate (PIP). Derivatives of Mg1 and Cs1 were obtained by soaking each crystal form in 5 mM EMTS. Heavy atom positions for each form were determined from analysis of isomorphous difference Patterson maps. The required NCS relations, both within and between the different crystal forms, were determined from rotation functions (*18*) and translation functions (*19*), and were confirmed by the heavy atom locations (although EMTS binds to different sites in the Av1 and Cp1 crystals). Phases obtained from the Av1 derivative data were used to define molecular envelopes (*20*) and were then refined by iterative NCS averaging of the electron density in the different crystal forms (*21*). Although the Av1 (*22*) and Cp1 (*23*) sequences are only ~36% identical, averaging between crystal forms was invaluable in the initial stages of the analysis. Polypeptide chains were built into the averaged density with the graphics program TOM (*24*) and refined with the restrained least squares program TNT (*25*). Phases calculated from the partial models were combined with the Av1 MIR phases and further averaged. Following several iterations of averaging, building, and refinement, the current model containing ~95% of the Av1 atoms has been obtained. At present, the R factor for this Av1 model is 0.197 to 2.7 Å resolution, although the fitting of the 2026 residues in the MoFe-protein tetramer is not yet final. Although a detailed description of the complete MoFe-protein structure is forthcoming, the α and β subunits exhibit homologous polypeptide folds that consist of three domains of the α/β type. Of particular interest for the

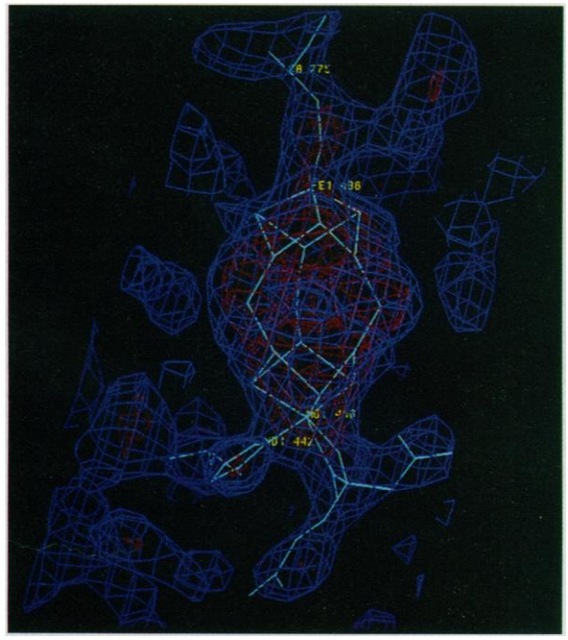

Fig. 1. Electron density map calculated at 2.8 Å resolution with superimposed FeMo-cofactor model. The map was generated by phase combination of the MIR and model phases, followed by NCS averaging in the Av1 crystal form. The blue and red densities are contoured at 2 and 4.5 times the standard deviation of the electron density map, respectively.

Table 1. Data processing and phasing statistics. Crystal form lists the type of crystal (native or derivative), with number of crystals used for data collection. Reflections with $I > 0$ measured to the limiting resolution were reduced to the unique data, with R_{merge} describing the agreement between symmetry-related reflections. The completeness of each data set to the limiting resolution is indicated as the percent of the theoretical number of reflections; ⟨m⟩ and pp describe the mean figure of merit and phasing power, respectively, associated with MIR phase calculations to 3.5 Å resolution.

Crystal form	Crystals (no.)	Resolution (Å)	R_{merge}	Complete reflections (%)	⟨m⟩	pp
Av1						
Native	2	2.75	0.085	94	0.62	
EMTS1	1	3.2	0.057	83		1.79
EMTS3	3	3.0	0.086	91		1.71
PTCL3	3	3.0	0.090	89		1.26
PIP3	3	3.0	0.111	92		1.17
Mg1						
Native	3	3.0	0.070	78	0.36	
EMTS	1	3.2	0.090	67		1.37
Cs1						
Native	3	3.0	0.084	74	0.35	
EMTS	1	3.2	0.087	64		1.37

present discussion, the subunits in an αβ pair are approximately related by a twofold rotation, although this axis does not intersect the tetramer twofold.

The redox centers were identified as the strongest features in the electron density map and are consistent with the highest peaks in both native anomalous difference Patterson and Fourier maps. As native anomalous scattering effects were not used in the phasing of the MoFe-protein structure, the initial electron density maps are not influenced by any specific model for the centers. Models for the centers were built into the electron density maps with fragments of 4Fe:4S clusters as the basic building blocks. Metal-ligand distances were restrained to values observed in model compound structures (*26*). The FeMo-cofactor and P-cluster were identified from the positions of amino acid residues that have been deduced from mutagenesis studies to be in the cofactor environment, including residues α275 and α195 for FeMo-cofactor and residues α62, α88, α154, β70, β95, and β153 for the P-cluster (*27–31*). At 2.7 Å resolution, atoms are not resolved, so that the identities of the various sites were inferred from the available analytical and spectroscopic information. The Mo site in the FeMo-cofactor was assigned to the position in the more electron dense cluster with approximate octahedral coordination geometry, as observed in extended x-ray absorption fine structure (EXAFS) studies (*32*), although octahedral iron coordination in 4Fe:4S clusters has also been observed (*33*). It should be emphasized that at this stage the proposed cluster models are consistent with the general shape and features of the electron density map, but the unambiguous identification of individual atoms, including the possible presence of hydrides, and a more detailed description of the geometry and oxidation states would require higher resolution diffraction data of both the MoFe-protein and isolated cofactors.

The electron density map surrounding the FeMo-cofactor is illustrated in Fig. 1, with the cofactor model built into this density presented in Fig. 2. The FeMo-cofactor model contains two clusters of composition 4Fe:3S and 1Mo:3Fe:3S that are bridged by three non-protein ligands. Compounds containing 4Fe:3S cluster fragments have been described (*34*), although the terminal ligation of the Fe sites in these molecules differs significantly from that observed in the FeMo-cofactor. In the FeMo-cofactor, the Fe-Fe separation distance between bridged iron sites is about 2.7 to 2.8 Å, whereas the separation distance is ~3.8 Å between nonbridged iron sites on different cluster fragments (such as Fe2 to Fe5). Consequently, a cavity of diameter ~4 Å appears inside the cofactor between the two cluster fragments. Based on the electron density values at the bridging ligands, two are assigned as sulfur (presumably S^{2-}), while the third ligand has lower electron density and is presently modeled, perhaps somewhat fancifully, by a group containing one nitrogen. This site could be occupied by water, a dithionite derived species (*35*), a less well ordered sulfur or other possibilities, however. Homocitrate, which is an essential component of FeMo-cofactor (*8*), appears to be coordinated through hydroxyl and carboxyl oxygens to the Mo. If the threefold axes of the isolated 4Fe:3S and 1Mo:3Fe:3S clusters are superimposed, then the cluster is liganded to the protein through the metals (Fe1 and Mo) located on the threefold axis. The Fe1 and Mo sites are separated by ~7.5 Å. The protein environment around the FeMo-cofactor is primarily provided by the α subunit. $Cys^{\alpha 275}$ coordinates Fe1, whereas the Mo is liganded by the side chain of $His^{\alpha 442}$. Two other side chains, $His^{\alpha 195}$ and $Gln^{\alpha 191}$, are within 5 Å of Fe2 and Fe6, respectively, but do not appear at the present state of the crystallographic analysis to be directly liganded to the metals. The side chain of $Gln^{\alpha 191}$ does interact with one of the carboxyl groups of homocitrate. $Cys^{\alpha 275}$, $His^{\alpha 442}$, $His^{\alpha 195}$, and $Gln^{\alpha 191}$ are conserved in all known MoFe-protein sequences; additionally, mutagenesis studies have implicated $Cys^{\alpha 275}$ (*27, 29*) and $His^{\alpha 195}$ (*28, 31*) as involved in the binding of FeMo-cofactor to MoFe-protein. Substitution of $Gln^{\alpha 191}$

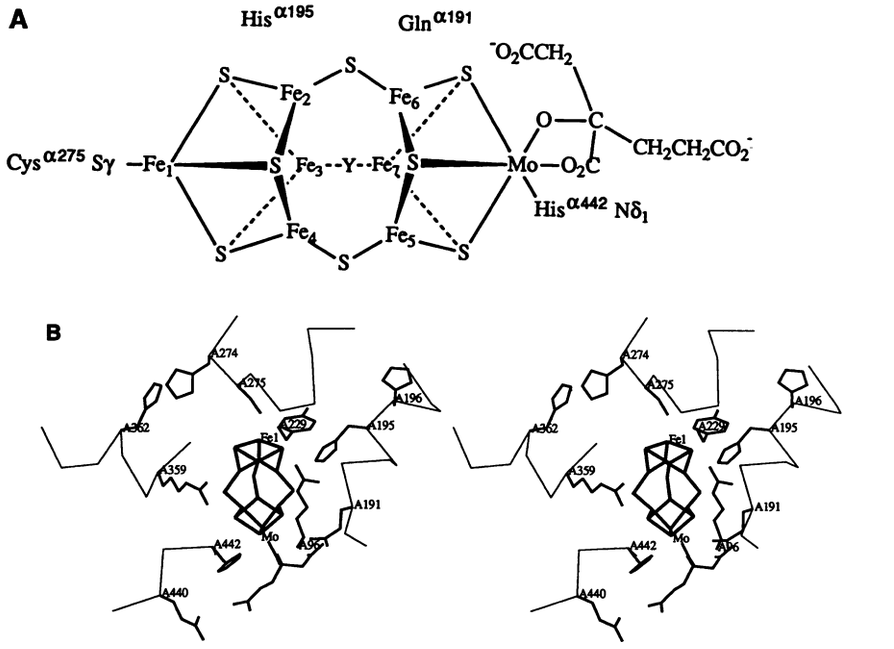

Fig. 2. (**A**) Schematic representation of the FeMo-cofactor model. Y represents the bridging ligand with relatively light electron density. (**B**) Stereoview of the FeMo-cofactor and surrounding protein environment.

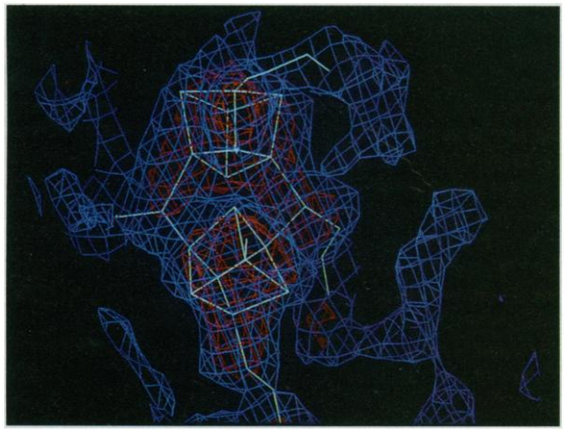

Fig. 3. Electron density map calculated at 2.8 Å resolution with superimposed P-cluster model. The map was generated by phase combination of the MIR and model phases, followed by NCS averaging in the Av1 crystal form. The blue and red densities are contoured at 2 and 4.5 times the standard deviation of the electron density map, respectively.

by Lys alters the substrate reduction properties of nitrogenase (36), and the present observations support the proposal that $Gln^{\alpha 191}$ interacts with homocitrate (36).

The tetrahedral coordination geometry of Fe1 and the octahedral coordination geometry for Mo are typical of the coordination environments for these metals observed in model compounds and Fe:S proteins (3, 26). An unusual feature of the FeMo-cofactor model, however, is the approximate trigonal planar geometry of the sulfurs surrounding the remaining six Fe sites that bind the bridging ligands. Solvent molecules that might possibly serve as fourth ligands have not been observed, and hydride species could never be identified in this type of x-ray diffraction experiment. There is also no evidence in the electron density maps for a hexacoordinate sulfur atom at the center of the cluster. Trigonal coordination geometry for Fe is not unprecedented and has been described in a small molecule structure of an Fe-thiolate species (37). In this case, the coordinating thiols contained bulky substituents, and it was proposed that the low coordination number of the Fe atoms reflected the effects of steric crowding between the ligands. Although the FeMo-cofactor does not contain bulky, non-protein groups, apparently the environment provided by the MoFe-protein produces a similar effect. The sensitivity of the isolated cofactor to the solvent type used for extraction and isolation (2) may reflect the properties of this category of Fe-sites in the FeMo-cofactor.

The structural features of the FeMo-cofactor model are generally consistent with the results of analytical and spectroscopic [EXAFS, electron nuclear double resonance (ENDOR), and Mössbauer] studies of the cofactor. The composition of the non-protein part of the FeMo-cofactor model, 1Mo:7Fe:8S:1 homocitrate, is within the range of values that have been reported (2, 7, 8), although this information was used in constructing the model, particularly in the assignment of the bridging ligands. The absence of protein-bound bridging ligands between the two clusters in FeMo-cofactor is consistent with the ability to extract the intact cofactor from MoFe-protein. EXAFS studies of the Mo environment in both the MoFe-protein and isolated cofactor indicate that two to three O or N atoms and three to five S atoms are directly coordinated to Mo, with three to four Fe atoms present in the second coordination shell of Mo (32); the crystallographic model contains three O or N atoms, three S atoms, and three Fe. Studies of Fe EXAFS on the isolated cofactor (38) indicate that, on average, each Fe atom is surrounded by ~3 S and 0.8 Mo (~2.7 Å), with ~2.2 and ~1.3 Fe atoms located at ~2.7 and ~3.8 Å, respectively. The average Fe environment in the present FeMo-cofactor model bound to the MoFe-protein (including protein ligands, and assuming that ligand Y is an O- or N-containing species) contains 2.9 S, 0.4 Mo, and 0.3 N (or O atoms), with 3.4 and 1.7 Fe atoms located at ~2.7 and ~3.8 Å, respectively. ENDOR studies with ^{57}Fe (39) have indicated that five magnetically inequivalent Fe species are present; neglecting the asymmetric protein environment and the chiral homocitrate ligand, five different types of Fe sites are observed in the structural model (Fe1, Fe3, Fe7, Fe2 and Fe4, and Fe5 and Fe6). Mössbauer studies (10, 40) identified five to seven iron sites in the FeMo-cofactor that could be grouped into two sets; however, assignment of these sites to particular atoms in the FeMo-cofactor model cannot be made at present.

The electron density map surrounding a P-cluster is illustrated in Fig. 3, with the structural model built into this density presented in Fig. 4. The P-cluster model contains two 4Fe:4S clusters that are bridged by two cysteine thiol ligands (from residues α88 and β95), with the four remaining Fe liganded by singly coordinating cysteine thiols (from residues α62, α154, β70, and β153). The nonbridging cysteines coordinated to a specific 4Fe:4S cluster are from the same subunit. In addition to the cysteine ligands, $Ser^{\beta 188}$ is close to Fe6 and may be able to coordinate this site along with $Cys^{\beta 153}$. The coordination environment must be distorted from ideal tetrahedral geometry for both Fe6 (due to interactions with $Ser^{\beta 188}$) and Fe2 (possibly due to interactions with the mainchain of $Gly^{\alpha 185}$ to obtain satisfactory fits of the 4Fe:4S clusters to the electron density. Individual replacement of any of the six cysteines by alanine eliminates diazotropic growth of the mutant strains (27, 29, 30). Interestingly, a double mutant with the two bridging cysteines, α88 and β95, both substituted by alanine exhibits activity (27), which was interpreted as indicating that these residues are located at the αβ subunit interface. Some non-alanine substitutions for $Cys^{\alpha 88}$ and $Cys^{\beta 153}$ have been described that can still produce nitrogenase with low activity (27, 29, 30), possibly as a consequence of the substituted residue functioning as a cluster ligand, or through a structural rearrangement that allows a previously nonliganding group to coordinate the cluster.

As had been proposed from sequence comparisons and mutagenesis experiments, the P-cluster is located at the interface between the α and β subunits (27, 29). The approximate twofold symmetry of the P-cluster is reflected in the sequence similarities (41) and folding of the polypeptide chains for the α and β subunits in this region. The location of this metal center at the interface between two homologous subunits, with the coordination sphere provided by residues from both subunits, is not unique to MoFe-protein, and has been previously observed in bacterial photosynthetic reaction centers [(42), with the nonheme Fe liganded by residues from two homologous subunits] and the nitrogenase Fe-protein [(4), with the 4Fe:4S cluster liganded by residues from two identical subunits].

Mössbauer and extrusion studies indicated that the P-clusters contained 4Fe:4S clusters (9–12). The proximity of two 4Fe:4S clusters in each P-cluster was suggested from an analysis of anomalous scattering effects from Cp1 (13). The properties of the 4Fe:4S groups in the P-cluster differ in significant ways from "typical" 4Fe:4S clusters, however. The close spatial proximity of two 4Fe:4S clusters in MoFe-protein suggests that interactions between clusters might confer distinctive properties. Mössbauer studies (11) have identified three distinct classes of iron sites in P-clusters, designated Fe^{2+}, D and S, that are present in the approximate ratio of 4:10:2 in the MoFe-protein. Because the environment of each metal site is necessarily unique when coordinated to an asymmetric protein, it is not clear what effects distinguish the different Mössbauer classes, so that the assignment between P-cluster iron sites and Mössbauer classes has not yet been determined.

The protein environment in the vicinity of the FeMo-cofactor and P-clusters is illustrated in Fig. 5. As demonstrated by Bolin *et al.* (13), these centers are separated by ~19 Å, whereas the distances between centers on the other αβ subunit pair of the MoFe-protein are ~67 Å. The distance of closest approach between metal sites in FeMo-cofactor and P-clusters is ~14 Å and occurs between Fe3 of the P-cluster and the side of the FeMo-cofactor that faces the P-cluster. Interestingly, the two cysteines that can tolerate some substitutions with partial retention of activity [α88 and β153 (27, 29, 30)] are positioned on the side of the P-cluster furthest from the FeMo-cofactor. The α helix containing the P-cluster ligand $Cys^{\alpha 62}$ provides the most direct structural connection between the P-cluster and FeMo-cofactor. Both clusters are shielded from direct exposure to water by the surrounding protein.

Although a molecular-level description of dinitrogen reduction by nitrogenase cannot yet be provided, the structure and environment of the MoFe-protein metal centers suggests the following considerations are relevant to any proposed mechanism:

1) The approximate twofold symmetry

of the P-cluster and surrounding peptide could be important in binding interactions of the MoFe-protein with the symmetrical Fe-protein dimer.

2) The closest distance between the metal sites in the P-cluster and FeMo-cofactor, ~14 Å, suggests that the electron transfer rate (*43*) between these centers could be faster than the rate of nitrogenase turnover [~5 s^{-1} (*44*)].

3) The octahedral coordination of Mo in FeMo-cofactor suggests that the Mo does not directly participate in substrate binding, without the occurrence of either a change in coordination number or a change in liganding groups.

4) The importance of homocitrate to the substrate reduction mechanism (*8*) may arise from modulation of the redox properties of the coordinated FeMo-cofactor, by functioning in the protonation of intermediates, by participating in the electron transfer pathway between the P-cluster and FeMo-cofactor, or through a combination of all of these mechanisms.

5) The metal sites with low coordination number in FeMo-cofactor should be well suited for substrate binding and could represent sites for hydride formation (*1*). Given the rather open structure, it is possible that dinitrogen and other substrates may bind inside the FeMo-cofactor.

6) Neither the FeMo-cofactor nor the P-clusters are exposed to the surface, suggesting that substrate entry, electron transfer, and product release must involve a carefully regulated sequence of interactions between MoFe-protein, Fe-protein, and adenine nucleotides (*4*).

It is hoped that the structural models for the FeMo-cofactor and P-clusters of MoFe-protein described in this report may facilitate the development of a detailed understanding of the nitrogenase mechanism.

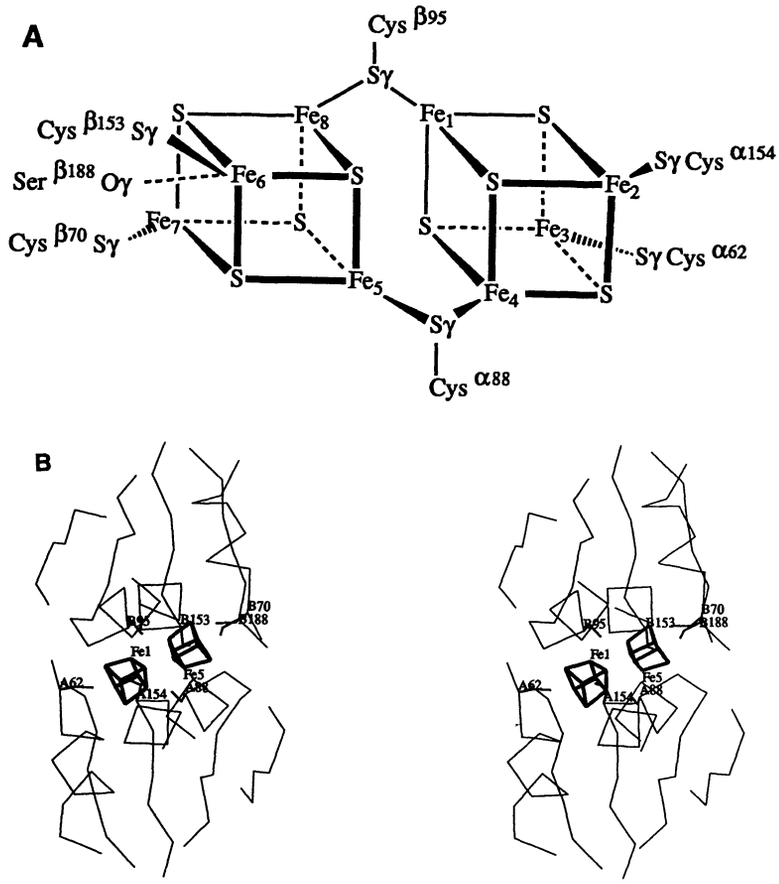

Fig. 4. (**A**) Schematic representation of the P-cluster model. (**B**) Stereoview of the P-cluster and surrounding protein model. The view is approximately along the direction of a twofold rotation axis approximately relating the α and β subunits.

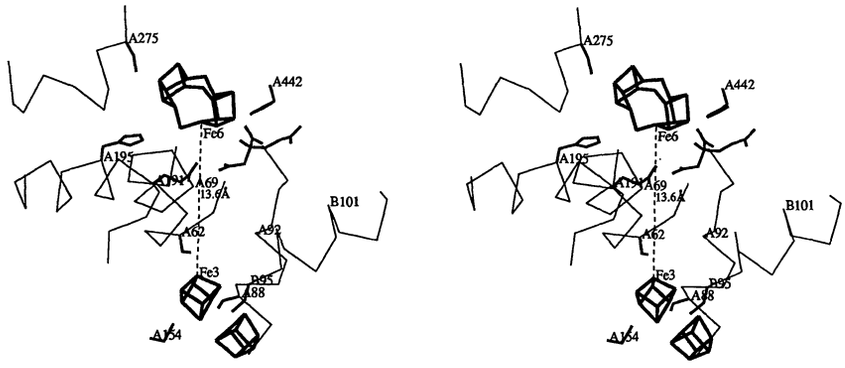

Fig. 5. Stereoview of the MoFe-protein structure in the vicinity of the FeMo-cofactor and P-cluster, including the Cα trace of the polypeptide chain and side chains of selected residues.

REFERENCES AND NOTES

1. B. K. Burgess, in *Advances in Nitrogen Fixation Research*, C. Veeger and W. E. Newton, Eds. (Nijhoff, Boston, 1984), pp. 103–114; W. H. Orme-Johnson, *Annu. Rev. Biophys. Biophys. Chem.* **14**, 419 (1985); R. H. Holm and E. D. Simhon, in *Molybdenum Enzymes*, T. G. Spiro, Ed. (Wiley-Interscience, New York, 1985), chap. 1; E. I. Stiefel *et al.*, *ACS Symp. Ser.* **372**, 372 (1988); R. H. Burris, *J. Biol. Chem.* **266**, 9339 (1991); B. E. Smith and R. R. Eady, *Eur. J. Biochem.* **205**, 1 (1992).
2. B. K. Burgess, *Chem. Rev.* **90**, 1377 (1990).
3. R. H. Holm, S. Ciurli, J. A. Weigel, H. Komiya, *Prog. Inorg. Chem.* **38**, 1 (1990).
4. M. M. Georgiadis, P. Chakrabarti, D. Woo, J. J. Kornuc, D. C. Rees, *Science* **257**, 1653 (1992).
5. V. K. Shah and W. Brill, *Proc. Natl. Acad. Sci. U.S.A.* **74**, 3249 (1977).
6. T. R. Hawkes *et al.*, *Biochem. J.* **217**, 317 (1984); J. Imperial *et al.*, *Biochemistry* **28**, 7796 (1989).
7. M. J. Nelson, M. A. Levy, W. H. Orme-Johnson, *Proc. Natl. Acad. Sci. U.S.A.* **80**, 147 (1983).
8. T. R. Hoover *et al.*, *Nature* **329**, 855 (1987); M. S. Madden, N. D. Kindon, P. W. Ludden, V. K. Shah, *Proc. Natl. Acad. Sci. U.S.A.* **87**, 6517 (1990).
9. D. M. Kurtz *et al.*, *Proc. Natl. Acad. Sci. U.S.A.* **76**, 4986 (1979).
10. R. Zimmermann *et al.*, *Biochem. Biophys. Acta.* **537**, 185 (1978); B. H. Huynh *et al.*, *ibid.* **623**, 124 (1980).
11. P. A. Lindahl *et al.*, *J. Biol. Chem.* **263**, 19412 (1988); *ibid.* **262**, 12900 (1987); K. K. Surerus *et al.*, *J. Am. Chem. Soc.*, in press.
12. W. R. Hagen, H. Wassink, R. R. Eady, B. E. Smith, H. Haaker, *Eur. J. Biochem.* **169**, 457–465 (1987).
13. J. T. Bolin *et al.*, in *Nitrogen Fixation: Achievements and Objectives*, P. M. Gresshoff, L. E. Roth, G. Stacey, W. E. Newton, Eds. (Chapman & Hall, New York, 1990), pp. 117–124.
14. B. K. Burgess, D. B. Jacobs, E. I. Stiefel, *Biochem. Biophys. Acta.* **614**, 196 (1980).
15. J. Drenth, W. G. J. Hol, R. K. Wierenga, *J. Biol. Chem.* **250**, 5268 (1975); M. M. Georgiadis, in preparation.
16. M. S. Weininger and L. E. Mortenson, *Proc. Natl. Acad. Sci. U.S.A.* **79**, 378 (1982).
17. A. J. Howard *et al.*, *J. Appl. Crystallogr.* **20**, 383 (1987).
18. M. G. Rossmann and D. M. Blow, *Acta Crystallogr.* **15**, 24 (1962); R. A. Crowther, in *The Molecular Replacement Method*, M. G. Rossmann, Ed.

(Gordon & Breach, New York, 1972), pp. 173–178.
19. R. A. Crowther and D. M. Blow, *Acta Crystallogr.* **23**, 544 (1967).
20. B. C. Wang, *Methods Enzymol.* **115**, 90 (1985).
21. M. G. Rossmann, Ed., *The Molecular Replacement Method* (Gordon & Breach, New York, 1972); G. Bricogne, *Acta Crystallogr.* **A32**, 832 (1976).
22. K. E. Brigle *et al.*, *Gene* **37**, 37 (1985).
23. S.-Z. Wang, J.-S. Chen, J. L. Johnson, *Biochemistry* **27**, 2800 (1988).
24. T. A. Jones, *Methods Enzymol.* **115**, 157 (1985).
25. D. E. Tronrud, L. F. Ten Eyck, B. W. Matthews, *Acta Crystallogr.* **A43**, 489 (1987).
26. T. Herskovitz *et al.*, *Proc. Natl. Acad. Sci. U.S.A.* **69**, 2437 (1972); D. Coucouvanis, *Acc. Chem. Res.* **24**, 1 (1991).
27. H. K. Kent *et al.*, *Biochem. J.* **264**, 257 (1989); H. M. Kent *et al.*, *Mol. Microbiol.* **4**, 1497 (1990).
28. D. J. Scott *et al.*, *Nature* **343**, 188 (1990).
29. D. R. Dean *et al.*, *Mol. Microbiol.* **4**, 1505 (1990).
30. H. D. May, D. R. Dean, W. E. Newton, *Biochem. J.* **277**, 457 (1991).
31. H. Thomann *et al.*, *J. Am. Chem. Soc.* **109**, 7913 (1987); H. Thomann, M. Bernardo, W. E. Newton, E. R. Dean, *Proc. Natl. Acad. Sci. U.S.A.* **88**, 6620 (1991).
32. M. K. Eidsness *et al.*, *J. Am. Chem. Soc.* **108**, 2746 (1986); S. D. Conradson *et al.*, *ibid.* **109**, 7507 (1987).
33. H. Lauble, M. C. Kennedy, H. Beinert, C. D. Stout, *Biochemistry* **31**, 2735 (1992).
34. C. T.-W. Chu and L. F. Dahl, *Inorg. Chem.* **16**, 3245 (1977).
35. B. Hedman *et al.*, *J. Am. Chem. Soc.* **110**, 3798 (1988).
36. D. J. Scott, D. R. Dean, W. E. Newton, in *Nitrogen Fixation: Achievements and Objectives*, P. M. Gresshoff, L. E. Roth, G. Stacey, W. E. Newton, Eds. (Chapman & Hall, New York, 1990), p. 169.
37. P. P. Power and S. C. Shoner, *Angew. Chem. Int. Ed. Engl.* **30**, 330 (1991).
38. J. M. Arber *et al.*, *Biochem. J.* **252**, 421 (1988).
39. A. E. True *et al.*, *J. Am. Chem. Soc.* **110**, 1935 (1988).
40. J. Rawlings *et al.*, *J. Biol. Chem.* **253**, 1001 (1978).
41. P. J. Lammers and R. Haselkorn, *Proc. Natl. Acad. Sci. U.S.A.* **80**, 4723 (1983).
42. J. Deisenhofer, O. Epp, K. Miki, R. Huber, H. Michel, *Nature* **318**, 618 (1985); J. P. Allen, G. Feher, T. O. Yeates, H. Komiya, D. C. Rees, *Proc. Natl. Acad. Sci. U.S.A.* **84**, 5730 (1987).
43. R. N. Marcus and N. Sutin, *Biochim. Biophys. Acta* **811**, 265 (1985); D. S. Wuttke *et al.*, *Science* **256**, 1007 (1992).
44. R. N. F. Thorneley and D. J. Lowe, *Biochem. J.* **224**, 887 (1984).
45. Discussions with J. B. Howard, J. E. Bercaw, and H. B. Gray and the assistance of M. M. Georgiadis, B. T. Hsu, D. Woo, A. J. Chirino, H. Komiya, D. Malerba, and M. K. Chan are gratefully appreciated. Supported by NSF grant DMB91-18689, with instrumentation funded in part by the Beckman Institute and the Joseph Irvine Equipment fund.

19 June 1992; accepted 18 August 1992

Threshold Phenomena and Long-Distance Activation of Transcription by RNA Polymerase II

Paul J. Laybourn and James T. Kadonaga*

To explore the underlying mechanisms by which genes are regulated in eukaryotes, long-distance transcriptional activation and threshold effects were reconstituted in vitro. Long-range activation of transcription by GAL4-VP16 protein located 1300 base pairs upstream of the RNA start site was dependent on packaging of the template into histone H1–containing chromatin. A transcriptional threshold effect by GAL4-VP16 was observed with repressed chromatin templates but not naked DNA templates. The experimental data with the chromatin templates were similar to the theoretical activation profile that is predicted if the action of each DNA bound protomer of GAL4-VP16 were independent and additive in terms of free energy.

The proper growth and development of an organism are dependent on a tiered array of processes by which genes are spatially and temporally regulated. Packaging and compaction of DNA render genes refractory to transcription, and the early stages in the pathway leading to gene activation appear to involve alterations in chromatin structure (*1*). Biochemical studies of RNA polymerase II transcription have revealed that basal transcription requires RNA polymerase II and several auxiliary factors (*2*), whereas the activity of the basal machinery is controlled by the combined action of sequence-specific DNA binding factors (*3*) and another class of factors known as coactivators or mediators (*4*). A major weakness of the biochemical experiments, however, has been the inability to recreate in vitro a number of phenomena that are observed in vivo. For instance, it has been difficult to achieve long-range activation of transcription, such as the action of enhancers in vitro (*5*). Moreover, threshold phenomena in which shallow gradients of transcription factors mediate sharp boundaries of gene activation have been well characterized in vivo (*6*) but not demonstrated in vitro for RNA polymerase II transcription.

In general, in vitro transcription experiments have been carried out with naked DNA templates, although reconstituted chromatin templates are probably a better model for the natural state of the DNA in the nucleus. To examine the role of chromatin structure in transcriptional activation, we have reconstituted and characterized chromatin templates prepared from purified components (*7*). Basal transcription is repressed with histone H1–containing chromatin, and the sequence-specific factors Sp1 and GAL4-VP16 both counteract the chromatin-mediated repression (antirepression) and facilitate the inherent transcription reaction (true activation). Thus, with transcriptionally repressed chromatin templates, transcriptional "activation" by a sequence-specific factor is the combination of both antirepression and true activation. Under such conditions of repressed basal transcription, the magnitude of transcriptional activation by Sp1 and GAL4-VP16 is similar to that observed in vivo.

Transcriptional enhancers are often key elements in the spatial and temporal regulation of genes, and the mechanisms by which enhancers activate transcription from relatively long distances (greater than 1 kb from the RNA start site) have been a subject of considerable investigation (*5*). As a first step in the biochemical analysis of enhancer function, we sought to reconstitute long-range activation of transcription. Typically, when the binding sites for sequence-specific factors are located more than 200 bp upstream of the RNA start site, the factors cannot activate transcription in vitro. There is, however, one report of long-range (1300 bp upstream of the start site) activation of transcription in vitro with the GAL4-VP16 hybrid activator protein (*8*). We attempted to reproduce this experiment but were not successful in recreating the long-distance activation (*9*). Although the molecular basis of this discrepancy in the data is not obvious, it is possible that the DNA template may have been assembled into a chromatin template in the previous study (*8*). Reconstitution of DNA into chromatin has been observed with in vitro transcription extracts (*10*), which contain histone H1, a repressor of RNA polymerase II transcription (*11*). We therefore examined the role of chromatin structure in long-range activation of transcription by GAL4-VP16.

In these experiments, the template DNAs were packaged into chromatin with purified components (with an average of one nucleosome per 200 bp and 0 to 1.5 molecules of histone H1 per nucleosome) (*7*) and then were transcribed in vitro (*12*). To examine long-range activation of transcription, we used a template DNA containing five tandem GAL4 binding sites located 1300 bp upstream of the adenovirus E4 promoter (pG5I1300AE4T) (*8*). In this simplified transcription factor–promoter system, long-distance transcriptional activation (antirepression) by GAL4-VP16 was

Department of Biology and Center for Molecular Genetics, University of California, San Diego, La Jolla, CA 92093.

*To whom correspondence should be addressed.